Desalination and Water Treatment
www.deswater.com
doi: 10.5004/dwt.2020.26386

205 (2020) 31–45
November

Systematic design of a wind-driven reverse osmosis desalination plant for Arar City, Saudi Arabia

Emad Ali

Chemical Engineering Department, King Saud University, Riyadh 11421, Saudi Arabia, email: amkamal@ksu.edu.sa (E. Ali)

Received 13 March 2020; Accepted 22 July 2020

ABSTRACT

Systematic design of a wind-driven reverse osmosis desalination plant is proposed. The desalination plant should supply 2,592 m^3/h of potable water to the inland arid city of Arar in the Kingdom of Saudi Arabia. For an annual average wind speed of 4.07, the numerical simulation indicated an optimum specific energy consumption occurs when the desalination plant operates at a 0.65–0.75 recovery ratio. The corresponding plant structure at this optimum condition comprises of 22 wind turbines and 500 membrane vessels. However, this plant failed to provide the city with enough water demand over a full year with an annual deficit of around 2,480–2,670 m^3/h because the monthly average wind speed fluctuates. Redesigning the plant structure using grid search over wind speed resulted in an optimum plant operation at a 0.75 recovery ratio with 19 wind turbines and 700 vessels. This plant configuration can sufficiently fulfill the city's annual water demand but at the expense of higher capital investment in terms of membrane vessels. It is also found that a tradeoff exists between the specific energy consumption and capital investment. Moreover, a tradeoff exists within the capital investment between the required number of turbines and vessels.

Keywords: Reverse osmosis; Wind; Desalination; Plant structure; Renewable energy

1. Introduction

Water is a viable natural resource found in abundance, however, supplying fresh potable water for a rapidly growing population and industrialization poses a challenge in several areas around the globe. This issue intensifies for arid and remote areas. Decision makers urge researchers and engineers to knockdown the problem with sustainable solutions. Potable water can be provided from different resources such as surface water, underground aquifers, and transportation from other regions. A review of water scarcity and resources is addressed in [1,2]. Water desalination is an alternative solution especially for regions that lack the other resources. Desalination of brackish water [3] and seawater [4] is considered the most widely used technology to supply water demand to areas suffering from water resource scarcity. However, the common dispute facing water desalination technologies is the high-energy consumption and adverse influence on the environment.

Reverse osmosis (RO) became the leading desalination technology as it shares 44% of the global desalination capacity and 80% of the overall deployed desalination plant [5]. RO is known for high salt rejection that reaches more than 99% [5]. More important, it is believed to inquire about the least energy demand among the several existing desalination methods. It is estimated that 3–6 kWh of electric power is needed to extract one cubic meter of pure water from seawater [6]. The major portion of the consumed energy is related to pressurizing the feed water. Yet, the cost of electric energy is vulnerable to fossil fuel prices. It is reported that a 25% fluctuation in energy cost can cause 11% variation in the specific water cost [7]. The electricity cost is estimated to be around 0.08 $/kWh [8,9], The water production cost for RO plants depends on its capacity and structure

with a range of 0.15–5.7 $/m^3$ is reported [9]. To avoid such cost fluctuations, it is recommended to operate desalination plants with renewable energy sources. Subsequently, integrated RO desalination systems with solar or wind energy became an attractive alternative that calls for growing attention. Several investigations dealing with integrating RO systems with renewable energy sources are reported in Ref. [10–12].

Saudi Arabia is an arid and swiftly developing country with a continuously increasing demand for freshwater and electricity. The nation power network provides electricity to a large portion of the population and areas. However, the country has a large surface area (2.3 million km^2), thereby, it is costly to connect all the remote regions to the power grid system. Subsequently, several isolated and sporadically populated areas need an individual source of power as well as potable water. These regions are in need of the use of renewable energy to generate electric power and to derive desalination plants. Moreover, the nation has the vision to reduce its reliance on fossil fuel and start establishing the appropriate infrastructure for renewable sources such as solar and wind energies. Based on the kingdom 2030 vision, it is planned to achieve a target of 58.7 GW from renewable energy resources which comprise 40 GW from solar PV, 13 GW from wind power, and 2.7 GW from concentrated solar panels [13]. Hence, there is a motive to leverage the available wind energy in these remote regions to produce freshwater from underground brackish water using RO technology. Despite, the different features of solar and wind energies, we adopt the wind energy source in this study. A recent wind speed survey in the kingdom indicated reasonable wind power with 75% of the surveyed area has an average wind speed higher than 3.5 m/s. In particular, Arar area reported and average wind speed of 4.5 m/s [13].

Globally, the utilization of wind energy to power RO units has been extensively studied. For example, Miranda and Infield [14] investigated the utilization of a small-scale wind-driven RO process for seawater desalination. They examined the system performance over wide operating conditions. Pestana et al. [15] conducted an experimental study on RO plant run by wind energy and energy storage. The plant can perform well over a wide range of operating conditions depending on the available power. Park et al. [16] investigated the impact of wind power fluctuation on the performance of the RO system for brackish water purification. They found that the proposed system can withstand wind speed variations for brackish water with low salt feed concentration. At high feed salinity, a suitable control policy must be implemented to achieve the desired quality product. Carta et al. [17], studied the design and operation approaches for a stand-alone wind-driven desalination unit. They found that RO technology can overtake the electrodialysis reversal technology and vacuum vapor compression technology even when linked with wind stations that were detached from the local energy grid. Recently, several types of research on hybrid RO-wind systems are reported. Charrouf et al. [18] proposed a power manager for the RO desalination plant using neural networks. The power manager ensures the transmission of smooth power to the plant by managing the generated power from three sources, solar panels, wind turbines, and battery banks. Peng et al. [19] used a state of the art optimization methods to design the size of a renewable-energy based desalination system. The system integrates solar panels, wind turbines, and reverse osmosis units. The optimization aims to provide continuous load while minimizing the life cycle of the system. Cabrera et al. [20] analyzed the performance of the seawater RO desalination plant powered by wind energy. The system is analyzed by three different machine learning approaches under fixed and variable feed pressure and flow rate. Lai et al. [21] proposed solution strategies to operate the RO desalination process under variable and intermittent wind energy. The solution strategies include using energy storage, hybridization with solar or geothermal energy sources, and adjusting the RO units and/or operating conditions. Carta et al. [22] studied the stand-alone RO desalination system powered by wind energy. The system is designed such that it adapts its energy consumption frequently to counter the fluctuation in the supplied power energy. Richards et al. [23] investigated the performance of the RO system for brackish water purification under real wind speed data. They concluded that the performance of the plant at constant average wind speed can provide insight on how the plant would perform under variable wind speed. The system is aided with a supercapacitor energy bank. Recent review papers on the integration of solar/wind energy with RO systems are given in Ref. [24,25].

As far as we know, not too much work has been reported to examine the performance of the RO desalination system for brackish water using wind power as the only source of energy. Moreover, wind energy is more suitable for RO desalination in a remote area as it is a green technology and its costs competitive with other energy sources [21]. According to Lai et al. [21], the cost of energy obtained from wind systems approaches 5–9 c/kWh onshore and 10–20 c/kWh offshore. According to Sims et al. [26] the energy cost-driven from fossil fuel ranges from 3.6 to 7.9, 3.9–8 c/kWh from nuclear, and 8.7–40 c/kWh from solar. This paper presents a scheme for designing the RO desalination plant for pure water production in Arar city (Northern province) of this country. The scheme helps to select an appropriate number of stand-alone wind turbines to power several vessels of reverse osmosis units. This work aims to assess the feasibility of harnessing the local wind power to operate the RO plant at the desired production capacity without the help of external electricity sources. In this case, a standalone wind-driven RO desalination plant will be studied. To supply the city with needed water demand despite the wind power variation, the proposed design will focus alternatively on meeting the annual production requirement instead of the hourly requirements. Therefore, the abundant water production during the period of high wind speed will be used to compensate for the losses during low-speed periods.

The paper is organized as follows. First, the mathematical equation that describes the RO system will be presented. Secondly, the numerical solution of the developed model for the RO system will be outlined. In the following section, the methodology to construct the integrated wind system and RO desalination plant will be described. Finally, the results of the system simulation will be discussed in the discussion section.

2. RO desalination unit production

In the following, we present the equations that describe the salt separation and permeate production rate in a typical RO membrane based on the transport mechanism of solute and solvent at a steady state, which is provided by Marriott and Sorensen [27].

For given pump power and feed pressure, the feed flow rate can be calculated from:

$$Q_f = \frac{3{,}600 \times P_w}{P_f \times 1 \times 10^5 \eta_p^{-1}} \tag{1}$$

where Q_f, P_f, P_w, and η_p are the feed flow rate, the feed pressure, wind power, and pump efficiency, respectively. For the assumed recovery rate (R_c), the permeate production rate (Q_p) is computed as follows:

$$Q_p = Q_f R_c \tag{2}$$

Mass balance around RO unit:

$$Q_f = Q_p + Q_c \tag{3}$$

$$Q_f C_f = Q_p C_p + Q_c C_c \tag{4}$$

where Q_c, C_c, and C_p are the brine flow rate, brine salinity, and permeate salinity, respectively. The flow rate of bulk fluid and its concentration are approximated by:

$$Q_b = \frac{Q_f + Q_c}{2} \tag{5}$$

$$C_b = \frac{C_f + C_c}{2} \tag{6}$$

The solvent volumetric flux, J_w, in terms of the membrane permeability (A) is given by [28]:

$$J_w = A\left(\Delta P - \Delta\pi\right) \tag{7}$$

where the following correlation for transmembrane pressure drop (DP) [28] is used:

$$\Delta P = P_f - P_b - P_{\text{drop}} / 2 \tag{8}$$

$$\Delta\pi = b_\pi \left(C_m - C_p\right) \tag{9}$$

In Eqs. (8) and (9), C_m is the salt concentration at the membrane surface and P_b is the brine outlet pressure. The osmotic coefficient, b_π, is defined as follows:

$$b_\pi = \frac{\pi}{C_b} \tag{10}$$

The osmotic pressure, π, is calculated using the following relationship:

$$\pi = 112T\sum \bar{m}_i \tag{11}$$

where $\sum \bar{m}_i$ is the sum of all modalities of dissolved ions (ppm) and T is the bulk temperature.

The pressure drop, P_{drop}, is given by the following correlation [28]:

$$P_{\text{drop}} = \lambda\left(\frac{Q_f + Q_c}{2 \times 3{,}600}\right)^a \tag{12}$$

In Eq. (12) $\lambda = 9.5 \times 10^8$ and $a = 1.7$.

The mass flux, J_s, of the solute in terms of the solute permeability (B) is given by:

$$J_s = B\left(C_m - C_p\right) \tag{13}$$

When the concentration polarization is present, the flux, J_w, at steady state, is given by [29]:

$$J_w = k_s \ln \frac{C_m - C_p}{C_b - C_p} \tag{14}$$

where k_s is the mass transfer coefficient. The solute flux is related to the solvent flux, as follows:

$$J_s = J_w C_p \tag{15}$$

The combination of Eqs. (10)–(12) and the elimination of C_m allows to obtain the following expression for the flux [30]:

$$J_w = A\left[\Delta P - b_\pi\left(\frac{BC_b \exp\left(J_w / k_s\right)}{J_w + B\exp\left(J_w / k_s\right)}\right)\exp\left(J_w / k_s\right)\right] \tag{16}$$

and

$$C_p = \frac{BC_b}{B + J_w \exp\left(J_w / k_s\right)} \tag{17}$$

Once the nonlinear algebraic Eqs. (1)–(17) is numerically solved, the permeate concentration, C_p, and the permeate production rate, Q_w are determined. The calculated production rate is defined as follows:

$$Q_w = J_w A_s n_e n_l \tag{18}$$

where A_s, n_e, and n_l are the membrane surface area, number of RO elements, and number of leaves per element, respectively. Also, to ensure the permeate salinity meet potability conditions, we constrain this concentration to be smaller than a desired specific value, C_{pd}:

$$C_p \le C_{\text{pd}} \tag{19}$$

Perforated baffles are used in spiral-wound membrane modules since they increase mass transfer. The following equation can be used to determine the mass transfer coefficient, k_s [31]:

$$\text{Sh} = 0.065\text{Re}^{0.865}\text{Sc}^{0.25} \tag{20}$$

where

$$\mathrm{Sh}=\frac{k_s}{D_{\mathrm{AB}}};\ \mathrm{Re}=\frac{d_h u}{\mu};\ \mathrm{Sc}=\frac{\nu}{D_{\mathrm{AB}}} \tag{21}$$

Note, m, v, D_{AB} are the viscosity, kinematic viscosity, and diffusivity of water. d_h is the hydraulic diameter of the channel. The velocity (u) in the feed channel that contains baffle is given by:

$$u=\frac{Q_b}{wh_{\mathrm{sp}}\varepsilon} \tag{22}$$

where w is the membrane width and d_h, h_{sp}, and ε are the baffle parameters. The kinematic viscosity, v, for brackish water can be calculated through the following correlation [32]:

$$v=0.0032+3.0\times10^{-6}C_b+4.0\times10^{-9}C_b^2 \tag{23}$$

The value of diffusivity, D_{AB}, is estimated to be 5.5×10^{-6} m²/h.

The RO process performance is assessed by two metrics. The recovery ratio is defined as follows:

$$R_c=\frac{Q_w}{Q_f} \tag{24}$$

The specific energy required for the generation of 1 m³ of freshwater is provided by Park et al. [16]:

$$\mathrm{SEC}=\frac{Q_f P_f \eta_p^{-1}}{Q_p} \tag{25}$$

A spiral wound module hydraulic diameter depends on the specific surface area of the spacer, the void fraction, and the channel height. Table 1 shows the RO membrane specifications [33] used here.

2.1. RO model simulation

The above steady-state RO model is cast in the form of nonlinear algebraic equations. To simulate such a model, certain input parameters must be specified. The feed salinity, C_f is always fixed at the value for the local brackish water. Hence another three process parameters must be specified to fully solve the RO model either in backward or forward fashion. In backward mode, the recovery ratio, R_c, the production rate, Q_p, and the permeate salinity, C_p are specified to determine the required feed pressure, feed flow rate, and the associated power. In forward mode, the available wind power, P_w, the desired recovery ratio R_c, and the permeate salinity, C_p are specified to determine the required feed pressure and flow rate, and production rate. Since the available wind power is known, we adopt the forward solution mode. Thus, the feed pressure and flow rate as well as the production rate will be calculated by an iterative procedure to meet a predefined permeate quality, that is, the permeate salinity, C_p. This numerical solution can be explained by the following algorithm denoted as *S*1.

- Define all process parameters and operating conditions such as C_f, P_w, and R_c.
- Set $P_f=\pi C_f$.
- Compute Q_f and Q_p using Eqs. (1) and (2).
- Assume initial values for $C_p=C_p^0$ and $C_m=C_m^0$.
- Compute Eqs. (3)–(17).
- If $C_p-C_p^0<\varepsilon$ and $C_m-C_m^0<\varepsilon$, where C_m and C_p are computed from Eqs. (14) and (17), respectively, proceed to step 7, otherwise set $C_p^0=C_p$ and $C_m^0=C_m$ go back to step 5.
- Compute the recovery ratio from Eqs. (24) and (18) and denoted as R_c'.
- If $R_c'-R_c<\varepsilon$ and $C_p\le C_{\mathrm{pd}}$ go to step 10.
- Set $P_f=P_f+1$, go to step 3.
- Compute specific energy consumption (SEC) from Eq. (25), Stop.

The termination criterion is set to $\varepsilon=1\times10^{-4}$. Since R_c is a decision variable, the above algorithm can be repeated for any value for R_c. It should be noted that algorithm *S*1 may lead to suboptimal value for P_f. Thereby we also attempt solving the RO model using the optimization approach as described by algorithm *S*2 below. In addition, optimization allows setting a constraint on the feed flow rate to avoid exceeding the upper design limit.

- Define all process parameters and operating conditions such as C_f, P_w, and R_c.
- Solve the following optimization problem numerically:

$$\min_{C_p,C_m,P_f}\phi=\left(C_p'-C_p\right)^2+\left(C_m'-C_m\right)^2+\left(R_c'-R_c\right)^2$$

Subject to:

$$f(P_f, C_p, C_m)=0$$

$$C_p\le C_{\mathrm{pd}}$$

$$Q_f\le Q_{f\max}$$

where f represents the nonlinear algebraic Eqs. (1)–(17), C_m', C_p, and R_c' are computed from Eqs. (14), (17), (18), and (24). The upper limit of the feed flow rate, $Q_{f\max}$ is set equal to 15 m³/h [34].

Table 1
Geometric specification of membrane module [33]

Parameter	Value
Hydraulic diameter of channel, d_h (mm)	0.78045
Height of spacer channel, h_{sp} (mm)	0.593
void fraction of the spacer, e (porosity)	0.9
Length of membrane, L (m)	1
Width of membrane, W (m)	37
Active area of the membrane, A_e (m²)	37
Reference water permeability, A_0 (m³/h bar)	19.43×10^{-4}
Reference solute permeability, B_0 (m³/h)	78.55×10^{-5}

2.2. Wind-driven RO plant design methodology

It is desired to design the RO plant structure necessary to provide Arar city with the required water demand. A sketch of the proposed plant configuration is depicted in Fig. 1. This structure comprises a network of RO modules, water pumps, and wind turbines. Several wind turbines can be used to provide the necessary electrical power needed by the water pump. The latter is linked to a RO vessel that contains eight RO elements each of which has three leaves. Since the maximum permissible feed flow rate for a single RO module is 15 m^3/h [34], the required pump capacity is limited by this operational constraint. Accordingly, and due to other limitations, a single RO vessel cannot produce the required water demand of Arar city. Consequently, the global number of RO vessels (N_v) equals to the desired water production divided by the permeate production of a single vessel. Of course, it is assumed that all vessels are identical and operating at the same input conditions, thereby having exactly the same production rate. As a result, depending on the available wind speed, a single wind turbine cannot supply enough power for all vessels. In this case, to better utilize the available wind power, the required number of wind turbines (N_T) is controlled by pump capacity and the total required power to produce the desired water production of Arar city. Selection of the number of wind turbines, the global number of vessels, and the operating condition for each vessel will be sought in this study. Note that determining the number of vessels and turbines is not straightforward because they are interrelated and depend on the required feed pressure which not known ahead. Thereby, the design methodology will be iterative in nature as will be discussed in the next section. Noting the population of Arar city in 2020 is estimated to be around 311,070 [35]. This value is a projection of the latest census data in 2014 using an annual growth rate of 6.41%. Census statistics for several cities in Saudi Arabia can be found in Ref. [36]. Setting the nominal water consumption per person to 200 L/d, the hourly water demand of Arar city is estimated to be 2,592 m^3/h.

As far as the wind power is concerned, the wind speed data for Arar city is given in Table 2 [36]. Table 2 lists the monthly averaged wind speed for the year 2015. We consider the wind speed pattern is almost similar every year. Updated wind speed data can also be found in commercial web sites such as whethearonline.com, whethearspark.com, etc. the long term averaged wind speed for Arar is reported by Alawaji et al. [37] to be 4.4 m/s. The average wind speed over a year is estimated here using the given data in Table 2 to be 4.07 m/s. The generated average wind power can be computed using the following correlation [38,39]:

$$P_w\left(\text{kW}\right)=\frac{1}{2}\rho C p_r A_r V^3 \tag{26}$$

Using the above correlation, the available average wind power is around 44 kW assuming 100% efficiency. This existing wind power and the desired water demand of Arar city set the basis for the design of the RO plant configuration. The baseline design specifications and constraints are listed in Table 3. It should be noted that in this study we present a general grassroots methodology for designing RO plant powered by wind speed. Since this is a grassroots design methodology, it is based on steady-state conditions where the wind speed is taken as a fixed average value over the year. The method can be straightforwardly applied to any updated values for the design parameters such as the city population, average wind speed, and power turbine efficiency. The penalty of using fixed wind speed will be tested by operating the plant under mild wind variation. This test is preliminary to explore the advantages and pitfalls of the design methodology. Rigorous analysis of the system operation under severe hourly wind fluctuation considering physical operational constraints and the effect of the process dynamics will be considered in upcoming research work.

3. Results and discussion

3.1. Preliminary design

First, we examine the behavior of a single RO vessel driven by a single wind turbine for demonstration purposes. For the given annually-averaged wind speed of 4.07,

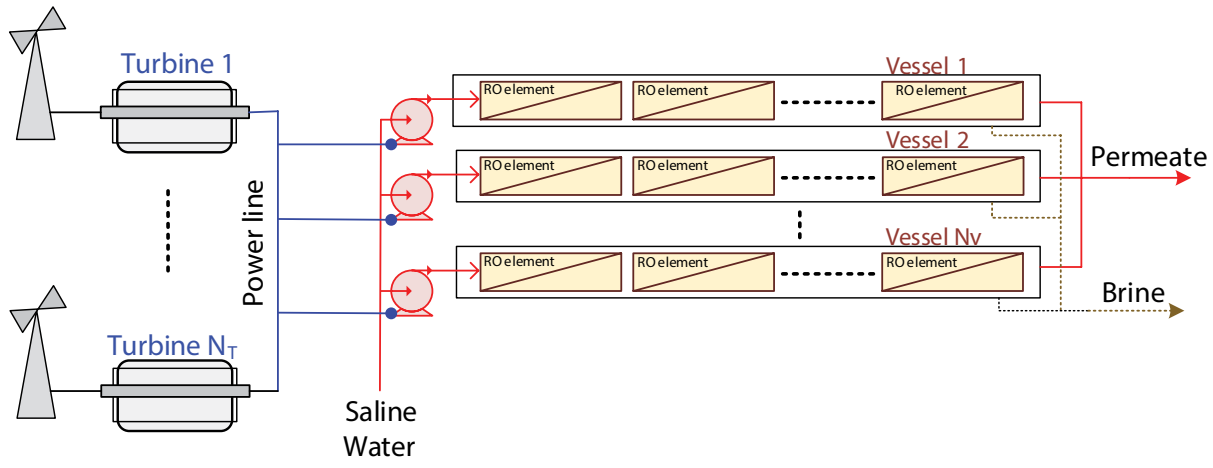

Fig. 1. Wind-driven RO plant structure.

Table 2
Wind speed data for Arar city [36]

Month	Knots	m/s
January	7	3.60
February	7	3.60
March	7	3.60
April	6	3.08
May	7	3.60
June	9	4.63
July	9	4.63
August	9	4.63
September	9	4.63
October	9	4.63
November	8	4.11
December	8	4.11

Table 3
Design specifications and constraints

Annual avergae wind power	44 kW
Arar city water demand	2,592 m^3/h
Brackish water salinity	1.0 kg/m^3 [41]
Maximum feed flow per vessel	15 m^3/h [34]
Minimum brine flow	3 m^3/h [37]
Maximum permeate concentration	0.5 kg/m^3
Discharged brine pressure, P_b	1 bar
Maximum feed pressure, P_f	80 bar [37]
Maximum pressure drop	0.7 bar [37]
Number of RO elements per vessel	8 [28]
Number of leaves per RO module	3 [42]
Wind turbine swept area of rotor (m^2)	2,290 [43]

the corresponding wind power is 44 kW. We assume a single wind turbine with 44 kW power is available to derive a single RO vessel containing eight RO elements each of which has three leaves. Hence, we simulate the RO model for such wind power to understand the process behavior and determine the best operating condition in terms of the recovery ratio. In addition, the total number of vessels required to produce the desired production rate can be estimated which is equal to the total production divided by the water production per vessel. The process is simulated using algorithm *S*1 executed at different values of R_c. The result of the simulation is shown in Fig. 2. In this case, no limitation is imposed on the feed flow rate, Q_f for analysis purposes. Fig. 2a demonstrates how to feed pressure increases with the required recovery ratio. This is intuitive because the required pressure to overcome the osmotic pressure and attain desired water salinity grows to achieve a higher production rate, that is, recovery ratio. The corresponding feed flow rate, which is linked to the feed pressure via Eq. (1), decreases with the recovery ratio as depicted in Fig. 2b because the pump power is fixed by the wind power while the feed pressure is increasing. As the feed flow rate decreases with increasing recovery ratio, the water production per vessel, which is equal to the multiplication of the feed flow rate by the recovery ratio, goes through a maximum value of about 17.3 m^3/h as shown in Fig. 2c. This maximum occurs at a recovery ratio of 0.65–0.7. Consequently, the SEC goes through a minimum as illustrated in Fig. 2d. Note SEC is simply the pump power (wind power) divided by the production rate per vessel which explains why it has a convex shape. Lastly, the number of parallel vessels needed to collectively produce the desired total production rate is shown in Fig. 2e. The optimal number of vessels, in this case, is around 149. Note this call for corresponding 149 wind turbines each of which has a capacity of 44 kW assuming each turbine derives one vessel. However, these results are impractical because the delivered feed flow rate over the entire recovery ratios is above the physical limit of 15 m^3/h as depicted in Fig. 2b. This means the wind turbine of 44 kW delivers more power than needed by a single vessel. Therefore, the outlet power of a single wind turbine can be split over several water pumps such that the pump outcome flow rate does not exceed 15 m^3/h. In this structure, which is shown in Fig. 1, each water pump is connected to a single vessel. All vessels comprise the same number of RO elements and size. Determination of the number of subdivisions of the power of a single wind turbine and consequently its associated water pumps/vessels is not straightforward. This is because the power, feed flow rate, and required transmembrane pressure are linked together according to Eq. (1).

The selection of the number of vessels and hence the associated wind turbines is devious, especially it is an integer variable and that both are correlated. We will present a procedure to determine the RO plant structure. The procedure will be based on equal distribution of the power over the number of stages (vessels). Within the procedure, the required RO pressure is determined either via iterative approach (algorithm *S*1) or numerical optimization (algorithm *S*2). The idea is to find the best design procedure and the structure for the RO plant. The steps of the procedure for selecting the design structure based on the iterative approach is shown in Fig. 3 and denoted as *S*3. Here we need to determine N_v and N_T, but since they are interrelated, we fix N_v and iterates over N_T by an iterative procedure. In this case, the available wind power of all turbines is divided into equal values each of which derives a single pump operating on a single vessel. Since the vessel's sizes are identical and the operating power is equal for all vessels, only one vessel is simulated. The rest will have the same results. Since the number of vessels is independently fixed, different values can be tested to assess its effect on plant performance as depicted in Fig. 4. The figure illustrates the process performance over a range of recovery ratios at a selected number of vessels. Note we examined the effect of N_v starting from 250 and beyond because there is a lower physical limit on N_v imposed by the $Q_{f\max}$ and R_c. In fact, the minimum allowable N_v equals to $Q_p/Q_{f\max}/R_c$. For the tested range of R_c, that is, 0.35 to 0.85, the minimum permissible N_v ranges between 203 and 497. The required feed pressure and the associated feed flow rate for each identical vessel is depicted in Figs. 4a and b. The feed pressure for any number of vessels increases with the recovery ratio as expected and observed in Fig. 2a. Moreover, the

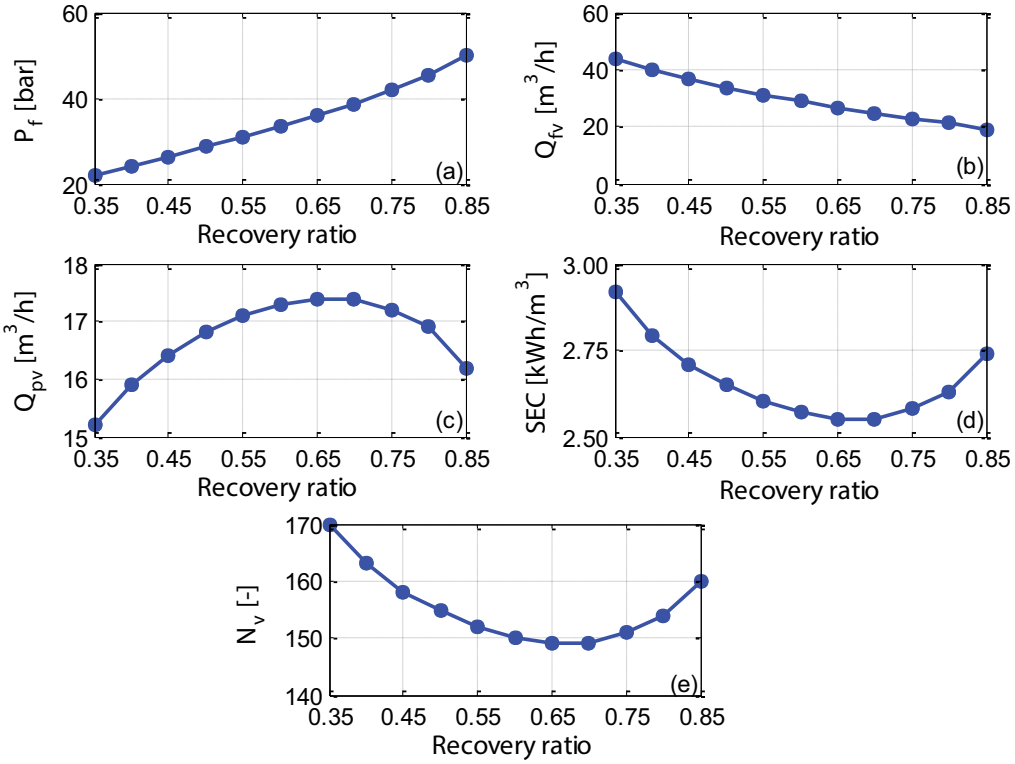

Fig. 2. Process simulation of a single vessel over a range of recovery ratio, P_w = 44 kW, C_f = 1.0 kg/m^3.

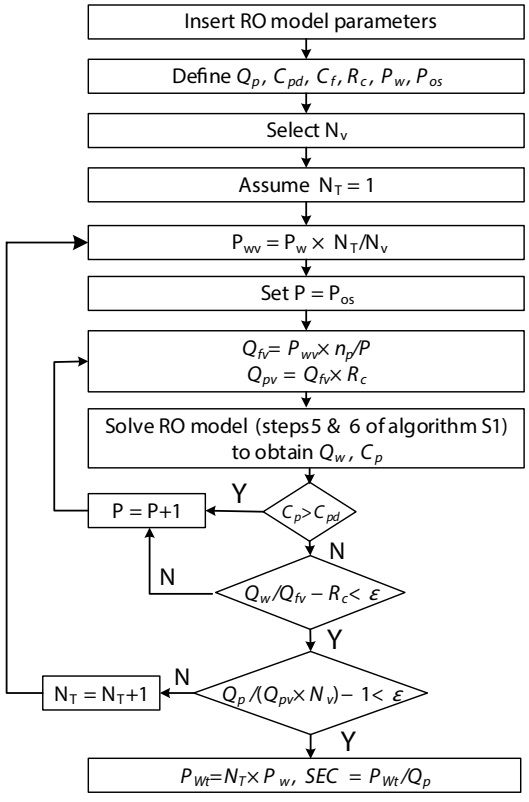

Fig. 3. Algorithm *S*3 organigram for designing the RO plant structure based on equal distribution of the wind power.

required feed pressure for a smaller number of vessels at any recovery ratio is higher than that needed for a larger number of vessels. At a low number of vessels, a significant amount of wind power is assigned to each pump causing a larger feed flow rate as shown in Fig. 4b. In due course, the greater feed pressure is needed to produce permeate with the desired salinity when operating at high feed flow rates. Fig. 4b demonstrates how the feed flow rate decreases with the recovery ratio because the feed pressure increases. Interestingly, the feed flow rate at a low number of stages particularly at N_v = 250, exceeds the upper operational limit almost over the entire tested recovery ratio except at R_c > 0.7. This situation is attenuated at a larger number of vessels (N_v), particularly when N_v equals 500 and beyond. Obviously, operation at a very low number of vessels and/or low recovery ratios may not be physically possible as feed flow rate may exceed the upper limit. As Fig. 4c illustrates, the number of turbines goes through an optimum around R_c of 0.65–0.75 with the optimum being smaller at a larger number of divisions (vessels). Note that the total production rate, that is, the sum of permeate rate of all stages, is greater when the number of divisions is larger incurring fewer turbines. N_T goes through an optimum because the vessel production rate has a concave trend as discussed earlier. The SEC follows the same trend of N_T because SEC is proportional to N_T. It is also clear that increasing the number of vessels beyond 500 has a little effect on N_T and SEC. It is clear that 500 is the minimum required vessels not because its lower the operation cost in terms of SEC and capital cost in terms of NT but also operates the plant at safe mode, This situation makes the overall SEC pass through a minimum

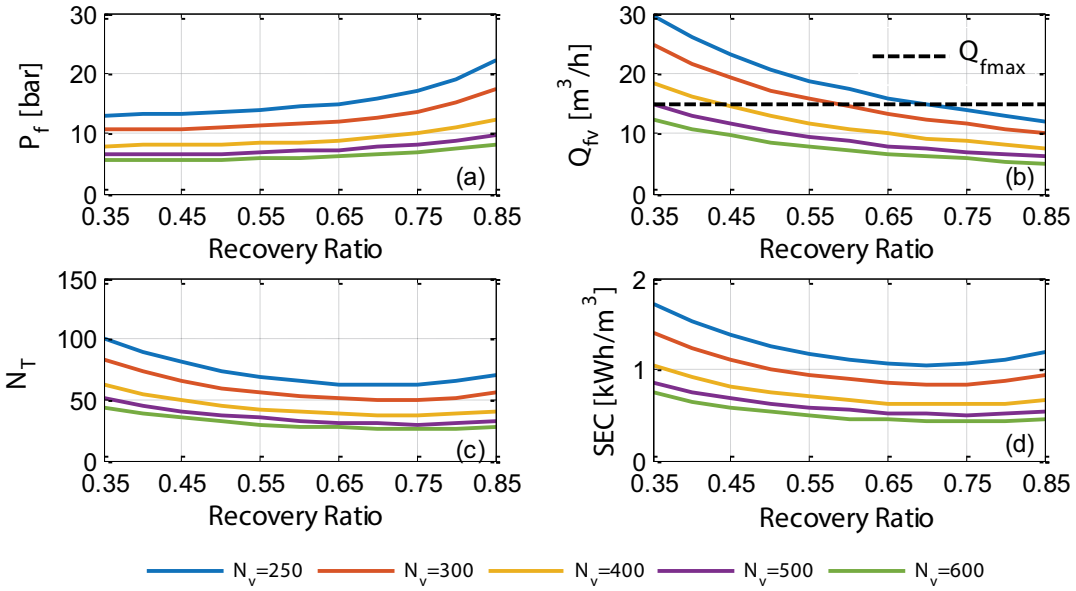

Fig. 4. Simulation results using algorithm *S*3.

around R_c range of 0.65–0.75 and high N_v. Therefore, this outcome suggests operating the RO plant at a recovery ratio of 0.65 with an optimum number of turbines of 31 and optimum SEC of 0.51 kWh/m³ for a global number of vessels of 500. This operating condition occurs at a minimum SEC but requires a larger investment in terms of the number of vessels. This is inevitable because lower values of N_v are restricted by the upper bound o the feed flow rate.

To further assess the results obtained by algorithm *S*3 we test algorithm *S*4. Besides, we expect algorithm *S*4 to find optimal values for the feed pressure and consequently the required power. This is because algorithm *S*3 excessively uses the feed pressure to satisfy two operating conditions, that is, permeate salinity and recovery ratio. The organigram of *S*4 is depicted in Fig. 5. The corresponding results are shown in Fig. 6. Note the results for N_v less than 400 are not shown because in these cases no feasible solution is found by algorithm *S*2. As seen in Fig. 4b, the obtained feed flow rate at low N_v exceeds the upper limit which violates the hard constraint imposed on Q_{fv} in algorithm *S*2. For the same reason, the results corresponding to N_v = 400 are reported fro recovery ratio equal and high than 0.45. The results are shown in Fig. 6, have the same trends obtained by algorithm *S*3. This result emphasizes the optimality of the overall SEC at R_c around 0.7–0.75 and a large value of N_v = 500. Therefore, it is of interest to select a higher value for N_v because it will likewise reduce the number of turbines slightly leading to lower capital investment. In fact, a trade-off between the N_v and N_t exists. The total equipment cost is controlled by the relative specific cost of the wind turbine and vessel. If the specific cost of the turbine is higher than that of a vessel, the number of turbines dominated the equipment cost and vice versa. At N_v of 500, the total number of needed turbines is 22 and SEC of 0.39 kWh/m³. The obtained SEC values are within the reported values [39]. We denote this plant design conditions as the reference case and it is defined in Table 4.

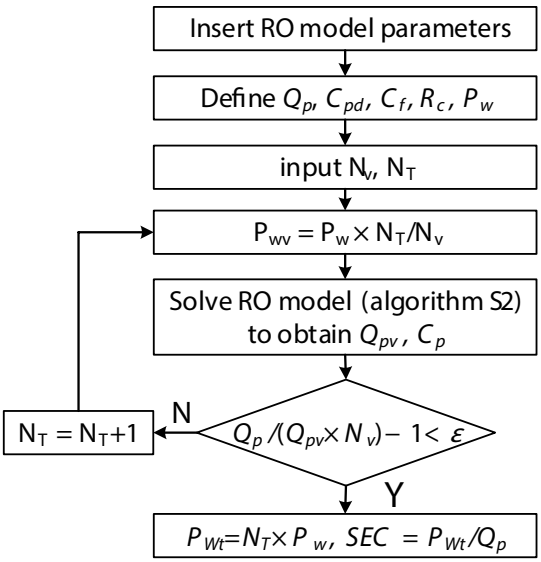

Fig. 5. Algorithm *S*4 organigram for designing the RO plant structure using equal power distribution and optimal operating conditions.

3.2. Testing the plant structure under wind fluctuation

Next, we examine the performance of the RO plant structure found in Table 4 during wind speed variation at different operating conditions. Indeed, the plant is simulated using the fluctuating wind speed listed in Table 2. The wind data in Table 2 can be categorized under three intervals. The low wind interval (months 1–5) where wind speed is below the annual average. The high wind interval (months 6–10) where the wind speed is higher than the annual average. The last 2 months where the wind speed is almost around the average value. Note the wind speed

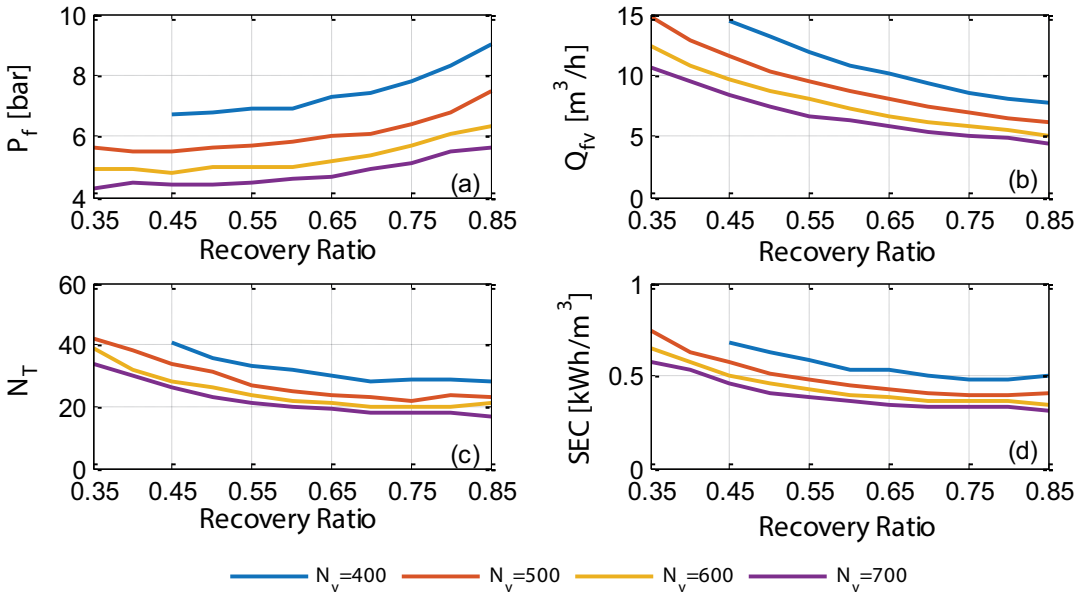

Fig. 6. Simulation result using algorithm *S*4.

Table 4
RO plant structure optimal parameters

Item	Annual average
V (m/s)	4.07
P_w (kW)	44
R_c	0.75
N_T	22
N_v	500
SEC (kWh/m^3)	0.39
Q_{pv} (m^3/h)	5.2
Q_{fv} (m^3/h)	6.9
P_f (bar)	6.4
C_p (kg/m^3)	0.45

is time-varying but the RO model is stationary. Hence, we consider the wind speed is stepwise constant, that is, constant over the month and changes only from month to month. Therefore, the RO model will be solved for each month independently assuming stationary conditions. Regarding the operating condition, we consider the feed salinity is increased to 1.6 kg/m^3 which represents the case when the salinity of the source is changed due to overuse or the underground source is changed. We also examine the case of a low recovery ratio which represents the case when the performance of the membrane degrades due to fouling or other reasons. Likewise, we examine the case of higher recovery ratio which represents the case when higher production is sought or when compensating the loss of production due to the shutdown of some vessels for maintenance. Simulating and comparing the plant performance at these operating conditions is depicted in Fig. 7. In this case, the RO model is simulated using fixed N_T, N_v, and P_f as given in Table 4 while the feed flow rate varies with alternating wind power. This means that the feed flow rate will increase at high wind speed and vice verse. Figs. 7a–c demonstrates the wind velocity, feed pressure, and feed flow rate for all cases. In the following we will discuss three cases; the lowest recovery ratio, the severe cases (R_c = 0.85 and C_f = 1.6 kg/m^3), and the nominal case (C_f = 1 kg/m^3 and R_c = 0.75) First, considering the case of lowest R_c, the production rate remains below the target throughout the year as shown in Fig. 7d. This is intuitive because we are operating the plant below the design point. During the low wind period, that is, month 1–5, the feed flow rate drops due to reduction in wind power, Since the feed pressure is fixed at baseline while feed flow became less than the baseline, the recovery ratio increases to 0.6 and the permeate salinity drops to 0.2 as depicted in Figs. 7e and f. On the other hand, during the high wind period, that is, month 6–10, the wind power grows and correspondingly the feed flow rate. In this situation, the fixed pressure at baseline was enough to maintain the required recovery ratio of 0.45. Secondly, for the severe cases, the production rate is reduced during the low wind period even if the required R_c is maintained. This is ascribed to the minimized feed flow rate through these months. As the wind speed becomes higher than the average, the corresponding production rate exceeds the target even that the recovery ratio falls below the designated values. This is attributed to the excess feed flow rate due to elevated wind power. Evidently, at an excess feed flow rate and fixed feed pressure, the process cannot keep the designated R_c and sacrifices the water quality as clearly shown in Figs. 7e and f. In fact, R_c drops and C_p hits the upper bound. Lastly, for the nominal case, the plant behavior at high wind interval follows that of the severe cases for the same reasons mentioned earlier. However, the permeate quality at low wind speed is different than the other cases especially the severe cases. At low wind power, the feed flow rate falls below the baseline while the feed pressure and recovery ratio are maintained at baseline points. Therefore, although

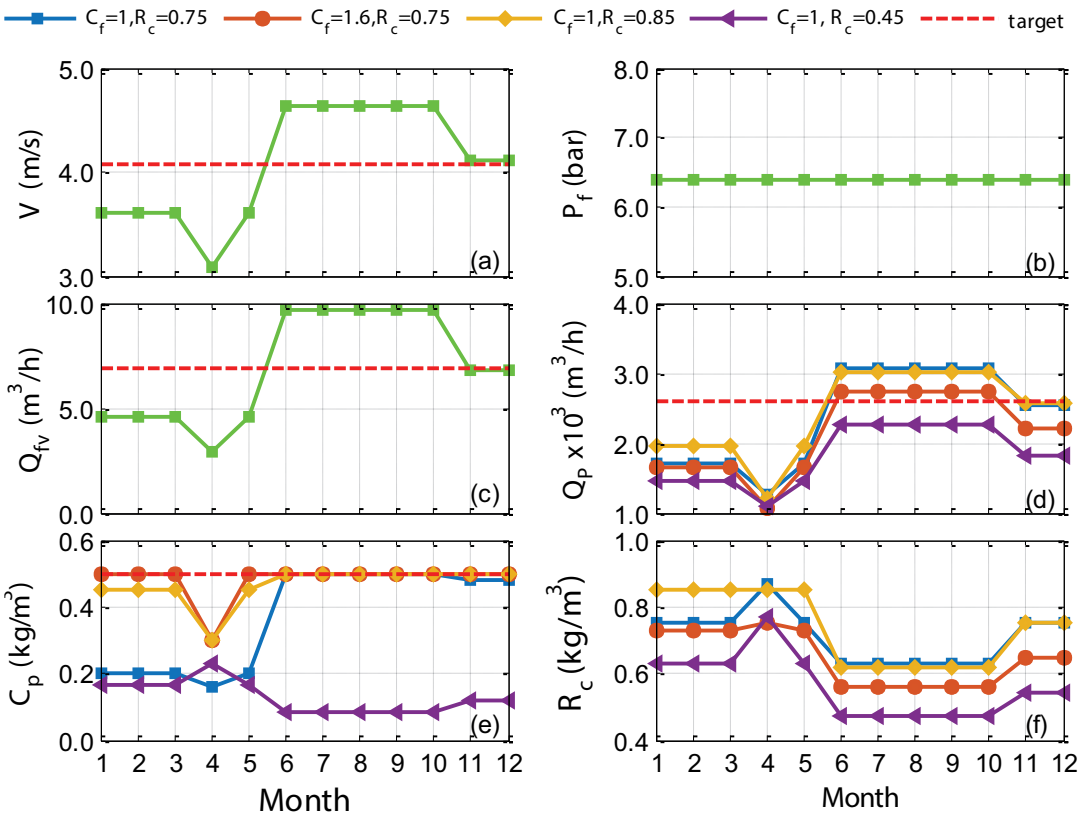

Fig. 7. Plant operation under different wind speeds and operating conditions, fixed P_f, N_T, and N_v.

P_f is at the baseline value, it can be considered relatively higher than that expected at a lower flow rate for the same R_c. As a result, the relatively spare pressure produces higher permeate quality, that is, less C_p value. When R_c is raised to 0.85 at fixed feed pressure at baseline, C_p can still be maintained within the design point because the feed flow rate is reduced. However, at C_f = 1.6, the permeate salinity can not be kept at design value even the feed flow rate is reduced because the feed salinity itself is much higher than the design point. In addition, it is noted in the 4th month a sudden drop in wind speed occurs causing a sudden drop in the feed flowrate. Consequently, the permeate salinity for the severe cases drops sharply because the constant feed pressure shifted toward enhancing the solvent mass transfer across the membrane as the recovery ratio is already satisfied. Oppositely, at the lowest recovery ratio, a little spike in C_p is observed because the excess feed pressure relative to the reduced feed flow rate shifted toward improving the recovery ratio since the permeate quality is already satisfied, that is, very low. More important is meeting the desired water demand. Accordingly, we computed the water balance (WB) For all cases. WB is the sum of the annual difference between the total permeated production of the plant and the target value. This can be computed as follows:

$$\mathrm{WB} = \sum_{i=1}^{12} \left(Q_{\mathrm{wt}}(i) - Q_P \right) \tag{27}$$

The numerical values for WB are listed in Table 5. Obviously, the plant experiences water deficit (negative values) throughout the year. This means the surplus water produced during high wind duration cannot compensate for the losses during the lower wind period.

We reexamine the above cases with feed pressure is allowed to vary in conjunction with the feed flow rate. This can be attained by using a control strategy to regulate the pressure as wind power departs from the nominal baseline. Here, we simply execute algorithm *S*4 for fixed plant structure (N_T, N_v) with feed pressure, and the flow rate is allowed to vary with alternating wind power. Carta et al. [22] proposed a similar approach, that is, variable pressure and flow rate, to adapt the power consumed by the RO vessels to the varying wind power. The result of this scenario is depicted in Fig. 8. In due course, both the pressure and flow rate varied with wind power as depicted in Figs. 8a and b. The overall trends illustrate a similar trend to those shown in Fig. 7 with some exceptions. The feed pressure is increased sufficiently to maintain the designated recovery ratio as shown in Fig. 8f for all cases. Also, the salinity of the permeate for the extreme cases as well as the nominal case can be maintained slightly lower than the upper limit by altering the feed pressure (Fig. 8e). For the lowest recovery ratio, the permeate salinity rises during the how wind period but still below the upper limit. For this case, the feed pressure became less than the baseline value which is enough to maintain the recovery ratio as low as 0.45.

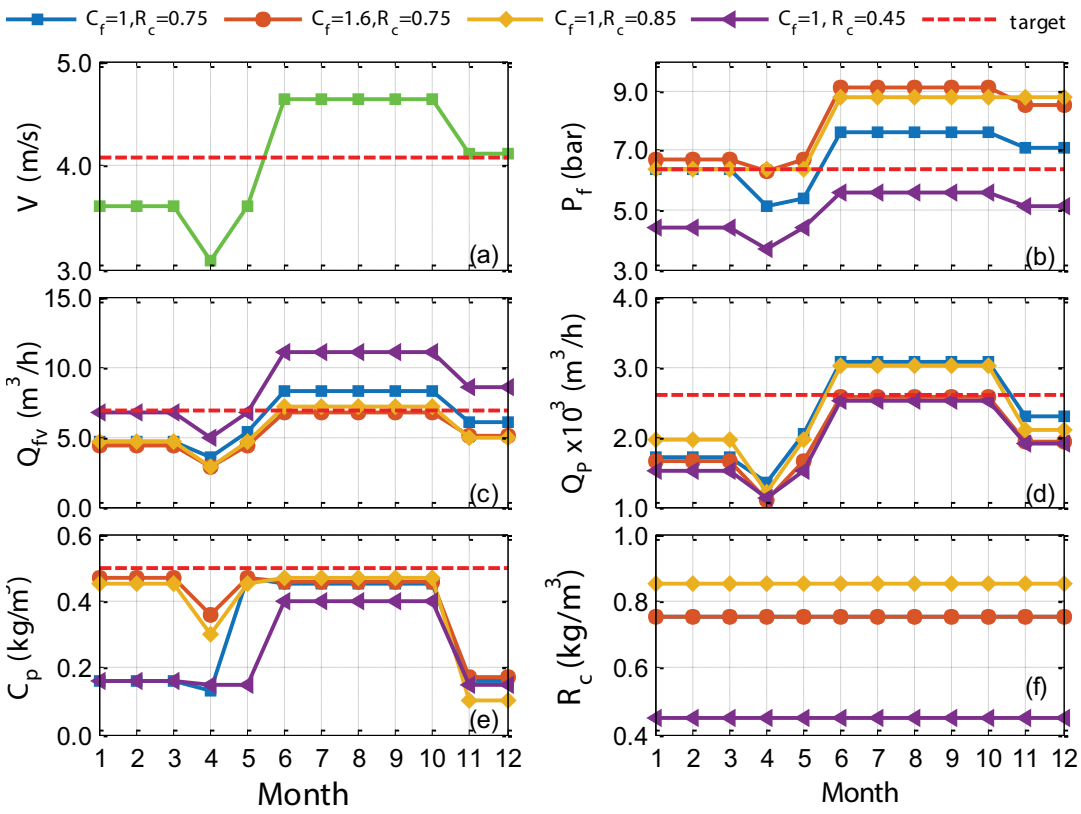

Fig. 8. Plant operation under different wind speeds and operating conditions, fixed N_T, N_v, and variable P_f.

As a result, the feed flow grew larger than that when the pressure is fixed (Fig. 7c) compromising the water purity. As noted before, a sharp drop in permeate salinity is observed in the 4th month for severe cases. As mentioned earlier this is due to the sharp drop in the feed flow rate while the feed pressure is kept high at least at the baseline value. This behavior is not observed for the baseline and the lowest R_c cases because the decline in feed flow rate is associated with a reduction in feed pressure, in addition, the solution salinity is far below the upper limit. To compare water surplus/deficit for the above two tests, Table 5 lists the sum of the difference between the target and the actual production over the entire year. It is obvious that both suffer from a deficit with the case of variable pressure being worse. This is because the elevated feed pressure in the second case was at the expense of lower feed flow rate and consequently production rate. Exception is the operation at the lowest recovery ratio where the deficit is less when P_f is variable. It is evident that both cases failed to provide Arar city with daily water demand. But we can consider operating at variable P_f is appealing because it results in better water quality. This is because the obtained plant structure depends on the chosen average wind speed. Thus, the plant should be redesigned such that it supplies the minimum water surplus throughout the year. This will be discussed in the following section.

3.3. Plant design by grid search

The wind speed plays an important role in plant design. Therefore, we will repeat the above design procedure for a range of values for the wind speed between 3 and 5 m/s. This range is chosen to encompass the minimum and maximum possible wind speed for Arar city as listed in Table 2. Since there are other effective decision variables such as R_c and

Table 5
Sum of the difference between the target and actual production rates over a year

Operating condition	$C_f = 1.0 \frac{kg}{m^3}$ $R_c = 0.75$	$C_f = 1.6 \frac{kg}{m^3}$ $R_c = 0.75$	$C_f = 1.0 \frac{kg}{m^3}$ $R_c = 0.85$	$C_f = 1.0 \frac{kg}{m^3}$ $R_c = 0.45$
Fixed P	–2,480.9 m³/h	–5,212.8 m³/h	–1,874.4 m³/h	–9,153.8 m³/h
Varible P	–2,671.3 m³/h	–6,818.9 m³/h	–2,845.8 m³/h	–7,624.2 m³/h

N_v, the procedure will be conducted under two schemes. In one scheme, wind speed and R_c are varied at fixed N_v while the other considers varying wind speed and N_v at fixed R_c. In order to assess and compare the plant design we select the following key performance indices (KPI), the total number of wind turbines (N_T), the average permeate quality (C_{pm}), the SEC, and the annual water balance (WB). This is attained by running algorithm *S*4 for several selected values for the design parameters, that is, V/R_c or V/N_v, and compute the KPI for each grid point. Note, N_T and SEC will be obtained directly by applying algorithm *S*4. However, C_{pm} and WB will be determined by further calculations. For example, at each grid point, the obtained N_T, N_v, and P_f will be used to simulate the plant over the whole year using the monthly average wind speed similar to that shown in Fig. 7. Of course, this can be also conducted at variable P_f as shown in Fig. 8. The grid search for V/R_c at a fixed N_v of 500 is illustrated in Fig. 9. In this case, variable P_f is used to determine WB and C_p. As far as the wind speed is concerned, V of 4 m/s provides the leats surplus WB as shown in Fig. 9a. This value is optimal because it meets the daily water demand over the entire year with extra excess water which can be stored for further need. Operating at a higher V value, the plant will undergo serious water shortages as WB becomes negative. Operating at a lower V value, the plant gain abundance of water surplus. This can be considered attractive because, during the high production period, part of the vessels can be shut down for maintenance or increasing the life cycle of the plant. However, this huge surplus is achieved at higher capital cost as N_T increase considerably. Interestingly, the wind speed has a minimal effect on SEC as shown in Fig. 9c. This is intuitive because SEC in Fig. 9 is the ratio of the total wind power to the fixed daily water requirement. Note that as wind speed varies, the number of turbines changes accordingly to maintain the total delivered wind power almost constant, that is, equal to that needed to produce the needed water hourly demand. Concerning R_c, it has a marginal effect on WB and N_T especially at high V but a remarkable impact of SEC. However, the reduction in SEC by increasing R_c from 0.75 to 0.85 is almost zero over the entire range of wind speed. This confirms our earlier findings. The water quality is shown in Fig. 9d indicates different profiles with acceptable value at V = 4 m/s. It reaches its best value at the lowest V and R_c while deteriorates at the highest R_c where it remains high over the entire range of wind speed. We can conclude that the plant design at N_v = 500, V = 4 m/s, and R_c = 0.75 is acceptable. This condition corresponds to N_T = 24, WB of 158 m^3/h, and SEC of 0.41 kWh/m^3. To emphasize the influence of fixed pressure operation on the plant performance, we repeat the above procedure with PF is fixed at the design point for each grid point during the calculations of WB and C_{pm}. The result is depicted in Fig. 10a. the other KPI are not shown because they lead to the same conclusion in Fig. 9. Evidently, the average permeates salinity becomes

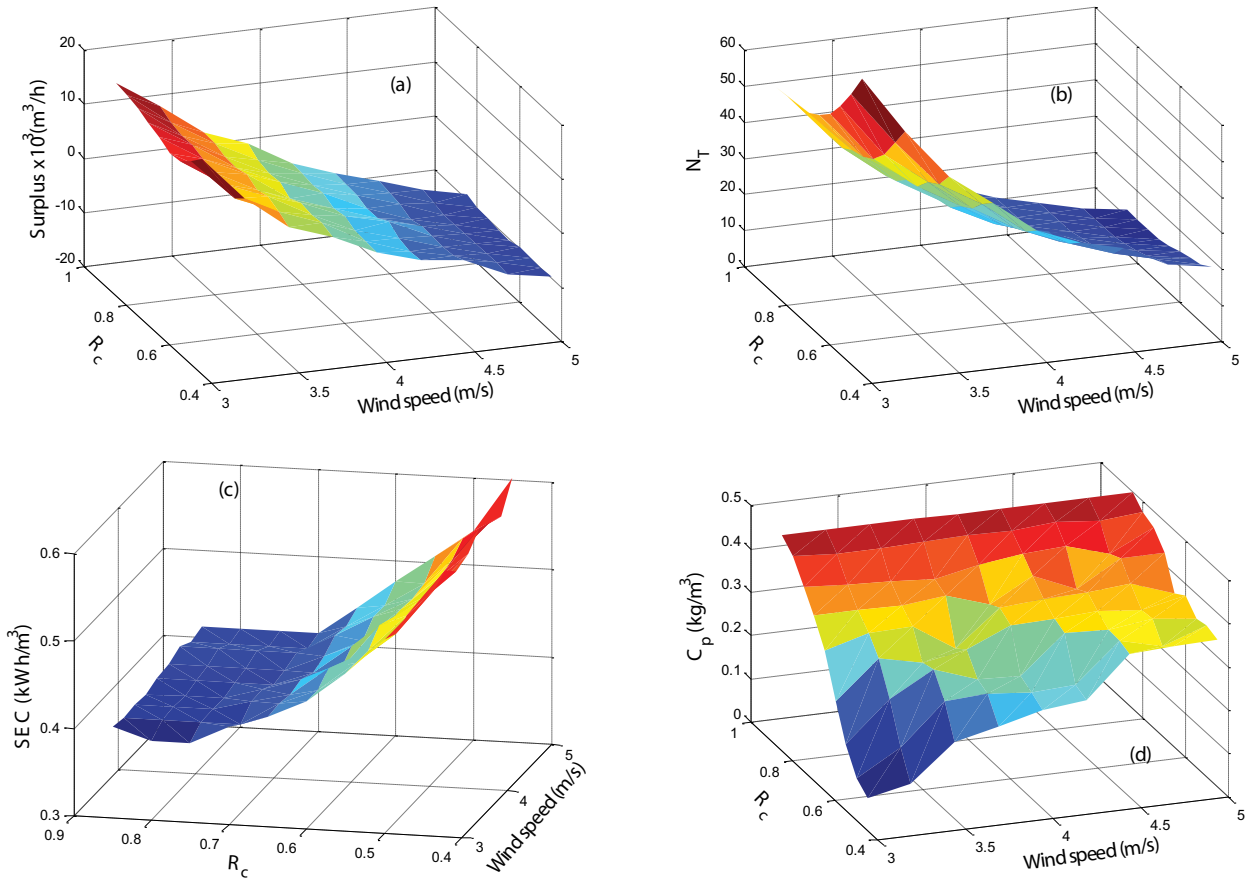

Fig. 9. KPI for plant design using grid search for V and R_c at fixed N_v = 500.

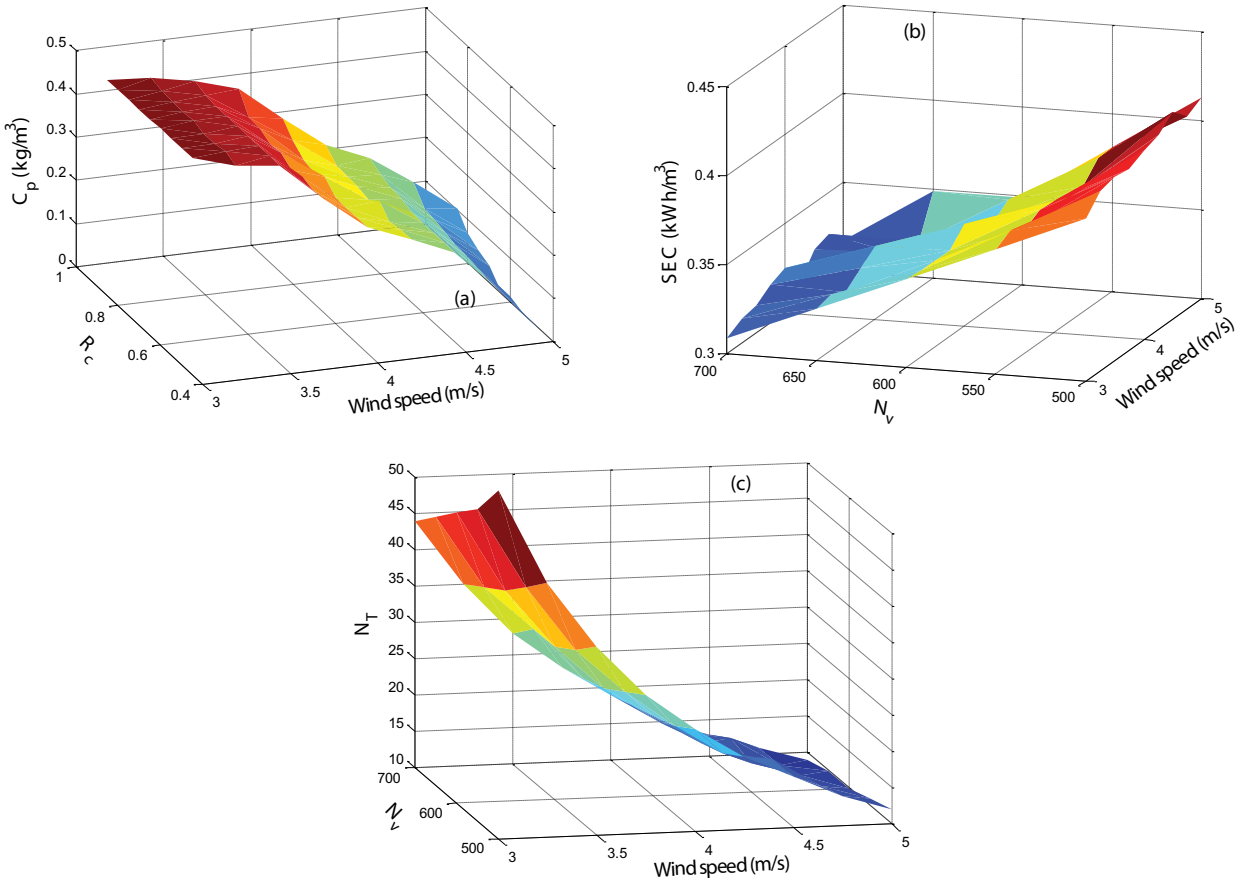

Fig. 10. KPI for plant design using grid search for (a) V and R_c at fixed N_v = 500 with fixed feed pressure, (b and c) V and N_v at fixed R_c = 0.75 with a variable feed pressure.

elevated at the lowest wind speed for any R_c and minimal at the highest wind speed for any R_c. Besides, we examined the plant design using V/N_v grid search at R_c of 0.75. The obtained result for SEC is shown in Fig. 10b using variable feed pressure. Again, the result for the other KPI is excluded for not providing significant changes from the earlier results. Obviously, N_v has a notable impact on SEC.

For fixed R_c of 0.75 and V = 4 m/s, SEC reduction resulted via increasing N_v from 500 to 700 is 20% with the mean SEC reduction over the entire wind velocities is 21.5%. This likewise is associated with further reduction in N_T by almost 20%. Therefore, the increment in capital investment due to increased N_v is balanced by a reduction in N_T. Consequently, depending on their relative specific cost, the design structure can also be promising. In due course, the design specification is V = 4 m/s, N_v = 700, N_T = 19, and R_c = 0.75. WB of 740 m^3/h and SEC of 0.33 kWh/m^3.

The previous analysis highlighted the dependence of the plant design on a trade-off between the operation cost manifested by the specific energy consumption and the capital fixed cost in terms of the required number of vessels. Indeed, the lower SEC occurs at higher N_v. Moreover, a compromise within the equipment fixed cost is underlined as a large number of vessels incurs a smaller number of wind turbines. The adverse impact of wind fluctuation is also underscored. The detrimental effect of wind fluctuation and intermittence on desalination plants driven by wind energy is well-known as several treatments were proposed by different researchers [18,21,23,40]. However, the scope here is focused on grassroots design. Plant improvements and remedies to withstand various types of wind alteration will be addressed in upcoming research work.

4. Conclusions

A systematic design of wind-driven desalination based on reverse osmosis technology is addressed theoretically. The desalination plant capacity should provide the daily potable water demand for a remote inland city of Arar in the kingdom of Saudi Arabia. Based on the city population and nominal daily water consumption, the hourly water demand for the city is estimated to be 2,592 m^3/h. A mathematical model for the RO process and numerical algorithms are used jointly to determine the desalination plant structure and operating condition. For the given city water demand and a local annual average wind speed of 4.07, the numerical methodology indicated the existence of a trade-off between the specific energy consumption and fixed capital investment. Considering SEC as the key criteria for the plant design, it is found that optimum operation occurs at a

recovery ratio of 0.75 incurring a total of 22 wind turbines and 500 RO vessels. The corresponding SEC is 0.39 kWh/m^3. Simulating the optimal RO plant structure using monthly variable wind speed indicated the inability of the proposed plant design to fulfill the required water demand over a whole year with an annual deficit of about 2,480–2,670 m^3/h depending on the operation strategy, that is, fixed feed pressure or adapted. The situation may worsen when the operating conditions change. Redesigning the desalination plant using a grid search over the possible wind speed range considering WB as the decision parameter resulted in an optimum SEC of 0.33 kWh/m^3 that corresponds to R_c of 0.76, total turbines of 19, and a total of vessels of 700. This plant configuration managed to supply the city with the desired water demand provided the water surplus produced during high wind speed is stored to offset the water deficit during the low wind period. Future work may include studying the effect of hourly changing wind power on the plant operation. Dynamic optimization and/or optimal control strategies may be implemented to overcome such variation.

Acknowledgment

This project is supported by the College of Engineering Research Centre, Deanship of Scientific Research, King Saud University.

Symbols

a	—	Coefficient for pressure drop correlation
A	—	Membrane permeability, m/h bar
A_r	—	Area swept by the rotor blade, m^2
A_s	—	Membrane surface area, m^2
B	—	Membrane solute permeability, m/h
b	—	Coefficient for viscosity correlation
b_π	—	Osmotic coefficient, m^3.bar/kg
C_f, C_p, C_c	—	Salt concentration in feed, permeate, and brine, kg/m^3
C_b, C_m	—	Average salt concentration and salt concentration at membrane wall, kg/m^3
C_{pd}	—	Desired salt concentration for permeate product, kg/m^3
Cp_r	—	Power coefficient for wind turbine
D_{AB}	—	Mass diffusivity, m^2/h
d_h	—	Hydraulic diameter of channel, m
h_{sp}	—	Weight of spacer channel, m
J_w	—	Water flux, m/h
J_s	—	Salts mass flux, kg/m^2 h
k_s	—	Mass transfer coefficient, m/h
m, m_i	—	Exponent in Eq. (2), molality of dissolved salt, ppm
N_T	—	Number of wind turbines
N_v	—	Global number of vessels
n_v	—	Number of vessels per turbine
N_p	—	Number of stages (pumps per turbine) which is equal to n_v
n_e	—	Number of RO elements in a vessel
n_l	—	Number of leaves per RO element
P_w	—	Average wind power, W
P_{wv}	—	Wind power per vessel, W
$P_{w\max}$	—	Wind power corresponding to maximum flow rate, W
P_f, P_b	—	Feed, permeate, and brine pressure, bar
P_{drop}	—	Pressure drop, bar
P_{os}	—	Osmotic pressure based on feed salinity, bar
Q_f, Q_p, Q_c	—	Feed, permeate, and brine volumetric flow rate, m^3/h
Q_b	—	Mean volumetric flow rate through membrane channel, m^3/h
Q_{fv}, Q_{pv}	—	Feed and permeate flow rate per vessel, m^3/h
Q_p	—	Water demand of Arar city, m^3/h
$Q_{f\max}$	—	Maximum allowable feed flow rate, m^3/h
Q_w	—	Production rate based on mass flux, m^3/h
Q_{wt}	—	Total plant production rate, m^3/h
R_c	—	Recovery ratio, %
Re	—	Reynolds number
SEC	—	Specific energy consumption, kWh/m^3
Sc	—	Schmidt number
Sh	—	Sherwood number
V	—	Wind speed, m/s
u	—	Velocity of water in feed channel, m/h
W	—	Width of the membrane, m
ρ	—	Air density, kg/m^3
ε	—	Termination factor also void fraction
η_p	—	Pump efficiency
π	—	Osmotic pressure, bar
λ	—	Coefficient for pressure drop correlation
ν	—	Kinematic viscosity
μ	—	Viscosity

References

[1] A. Gohari, S. Eslamian, A. Mirchi, J. Abedi-Koupaei, Al. M. Bavani, K. Madani, Water transfer as a solution to water shortage: a fix that can Backfire, J. Hydrol., 491 (2013) 23–39.
[2] S.N. Gosling, N.W. Arnell, A global assessment of the impact of climate change on water scarcity, Clim. Change, 134 (2016) 371–385
[3] G. Vlachos, J.K. Kaldellis, Application of a gas-turbine exhausted gases to brackish water desalination. A techno-economic evaluation, Appl. Therm. Eng., 24 (2004) 2487–2500.
[4] J.K. Kaldellis, K. Kavadias, J. Garofalakis, Renewable Energy Solution for Clean Water Production in the Aegean Archipelago islands, Mediterranean Conference on Policies and Strategies for Desalination and Renewable Energies, Santorini Island, Greece, 2000.
[5] L.F. Greenlee, D.F. Lawler, B.D. Freeman, B. Marrot, P. Moulin, Reverse osmosis desalination: water sources, technology, and today's challenges, Water Res., 43 (2009) 2317–2348.
[6] R. Dashtpour, S.N. Al-Zubaidy, Energy efficient reverse osmosis desalination process, Int. J. Environ. Sci. Dev., 4 (2012) 339–345.
[7] C.A. Charcosset, A review of membrane processes and renewable energies for desalination, Desalination, 245 (2009) 214–231.
[8] Y.-Y. Lu, Y.-D. Hu, X.-L. Zhang, L.-Y. Wu, Q.-Z. Liu, Optimum design of reverse osmosis system under different feed concentration and product specification, J. Membr. Sci., 287 (2007) 219–229.
[9] M.S. Atab, A.J. Smallbone, A.P. Roskilly, An operational and economic study of a reverse osmosis desalination system for potable water and land irrigation, Desalination, 397 (2016) 174–184.
[10] N. Ghaffour, S. Lattemann, T. Missimer, K. Choon, S. Sinha, G. Amy, Renewable energy-driven innovative energy-efficient desalination technologies, Appl. Energy, 136 (2014) 1155–1165.

[11] C.-S. Karavas, K.G. Arvanitis, G. Papadakis, Optimal technical and economic configuration of photo voltaic powered reverse osmosis desalination systems operating in autonomous mode, Desalination, 466 (2019) 97–106.
[12] M.A. Abdelkareem, M.E. Assad, E.T. Sayed, B. Soudan, Recent progress in the use of renewable energy sources to power water desalination plants, Desalination, 435 (2018) 97–11.
[13] M.M. Salah, A.G. Abo-khalil, R.P. Praveen, Wind speed characteristics and energy potential for selected sites in Saudi Arabia, J. King Saud Univ. Eng. Sci., (2020), doi: 10.1016/j.jksues.2019.12.006 (in press).
[14] M.S. Miranda, D.A. Infield, A wind-powered seawater reverse-osmosis system without batteries, Desalination, 153 (2002) 9–16.
[15] N. Pestana, F.J. Latorre, C.A. Espinoza, A.G. Gotor, Optimization of RO desalination systems powered by renewable energies. Part I: wind energy, Desalination, 160 (2004) 293–299.
[16] G.L. Park, A.I. Schafer, B.S. Richards, Renewable energy powered membrane technology: the effect of wind speed fluctuations on the performance of a wind-powered membrane system for brackish water desalination, J. Membr. Sci., 370 (2011) 34–44.
[17] J.A. Carta, J. Gonzhlez, V. Subiela, The SDAWES project: an ambitious R&D prototype for wind powered desalination, Desalination, 161 (2004) 33–48.
[18] O. Charrouf, A. Betka, S. Abdeddaima, A. Ghamri, Artificial neural network power manager for hybrid PV-wind desalination system, Math. Comput. Simul., 167 (2020) 443–460.
[19] W. Peng, A. Maleki, M.A. Rosen, P. Azarikhah, Optimization of a hybrid system for solar-wind-based water desalination by reverse osmosis: comparison of approaches, Desalination, 442 (2018) 16–31.
[20] P. Cabrera, J.A. Carta, J. González, G. Melián, Wind-driven SWRO desalination prototype with and without batteries: a performance simulation using machine learning models, Desalination, 435 (2018) 77–96.
[21] W. Lai, Q. Ma, H. Lu, S. Weng, J. Fan, H. Fang, Effects of wind intermittence and fluctuation on reverse osmosis desalination process and solution strategies, Desalination, 395 (2016) 17–27.
[22] J.A. Carta, J. González, P. Cabrera, V.J. Subiela, Preliminary experimental analysis of a small-scale prototype SWRO desalination plant, designed for continuous adjustment of its energy consumption to the widely varying power generated by a stand-alone wind turbine, Appl. Energy, 137 (2015) 222–239.
[23] B.S. Richards, G.L. Park, T. Pietzsch, A.I. Schäfer, Renewable energy powered membrane technology: Brackish water desalination system operated using real wind fluctuations and energy buffering, J. Membr. Sci., 468 (2014) 224–232.
[24] M.T. Mito, X. Ma, H. Albuflasa, P.A. Davies, Reverse osmosis (RO) membrane desalination driven by wind and solar photovoltaic (PV) energy: state of the art and challenges for large-scale implementation, Renewable Sustainable Energy Rev., 112 (2019) 669–685.
[25] M.A.M. Khan, S. Rehman, F.A. Al-Sulaiman, A hybrid renewable energy system as a potential energy source for water desalination using reverse osmosis: a review, Renewable Sustainable Energy Rev., 97 (2018) 456–477.
[26] R.E.H. Sims, H.-H Rognerb, K. Gregory, Carbon emission and mitigation cost comparisons between fossil fuel, Energy Policy, 31 (2003) 1315–1326.
[27] J. Marriott, E.A. Sorensen, A general approach to modelling membrane modules, Chem. Eng. Sci., 58 (2003) 4975–4990.
[28] F. Vince, F. Marechal, E. Aoustin, P. Bréant, Multi-objective optimization of RO desalination plants, Desalination, 222 (2008) 96–118.
[29] T.K. Sherwood, P.L.T. Brian, Fischer reverse desalination by reverse osmosis, Ind. Eng. Chem. Fundam., 6 (1967) 2–12.
[30] R. Rautenbach, Process Design and Optimization, P.M. Bungay, H.K. Lonsdale, M.N. de Pinho, Eds., Synthetic Membranes: Science, Engineering and Applications, Kluwer, New York, NY, 1986.
[31] A.R. Da Costa, A.G. Fane, D.E. Wiley, Spacer characterization and pressure drop modelling in spacer-filled channels for ultrafiltration, J. Membr. Sci., 87 (1994) 79–98.
[32] S. Sourirajan, Reverse Osmosis, Academic Press, New York, NY, 1970.
[33] N. Al-Bastaki, A. Abbas, Permeate recycle to improve the performance of a spiral-wound RO plant, Desalination, 158 (2003) 119–126.
[34] Hydranautics. Available at: https://membranes.com/docs/trc/Dsgn_Lmt.pdf (accessed February 14, 2020)
[35] Available at: http://population.city/saudi-arabia/arar/ (accessed February 14, 2020).
[36] General Authority of Statistics. Available at: https://www.stats.gov.sa/ar/3123 (accessed February 14, 2020)
[37] S.H. Alawaji, N.N. Eugenio, U.A. Elani, Wind energy resource assessment in Saudi Arabia: Part II: Data collection and analysis, Renewable Energy, 9 (1996) 818–821.
[38] NREL, Integrated Wind Energy/Desalination System. Available at: https://www.nrel.gov/docs/fy07osti/39485.pdf (accessed February 14, 2020)
[39] A.S. Stillwell, M.E. Webber, Predicting the specific energy consumption of reverse osmosis desalination, Water, 8 (2016) 1–18, doi: 10.3390/w8120601.
[40] W. Khiari, M. Turki, J. Belhadj, Power control strategy for PV/Wind reverse osmosis desalination without battery, Control Eng. Pract., 89 (2019) 169–179.
[41] A. Al-Naeem, Monitoring of groundwater salinity for water resources management in irrigated areas of Al-Jouf region, Saudi Arabia, Res. J. Environ. Sci., 9 (2015) 256–269.
[42] G. Srivathsan, Modeling of Fluid Flow in Spiral Wound Reverse Osmosis Membranes, Ph.D Thesis, University of Minnesota, USA, 2013.
[43] Z. Triki, Etudes Analyses et Optimisation de la Consommation Énergétique des Unités de Dessalement Pour les Sites Isolés, Ph.D Thesis, Universite of Constantine, Algeria, 2014.